Published in final edited form as:
Cancer Res. 2011 February 1; 71(3): 1050–1059. doi:10.1158/0008-5472.CAN-10-3091.

A Mammaglobin-A Targeting Agent for Non-invasive Detection of Breast Cancer Metastasis in Lymph Nodes

NK Tafreshi[1], **SA Enkemann**[2], **MM Bui**[3,4], **MC Lloyd**[4], **D Abrahams**[7], **AS Huynh**[1], **J Kim**[5], **SR Grobmyer**[8], **WB Carter**[6], **J Vagner**[9], **RJ Gillies**[1], and **DL Morse**[*,1]

[1]Dept. Functional & Molecular Imaging, H. Lee Moffitt Cancer Center & Research Institute, Tampa, FL

[2]Microarray Core Facility, H. Lee Moffitt Cancer Center & Research Institute, Tampa, FL

[3]Anatomic Pathology, H. Lee Moffitt Cancer Center & Research Institute, Tampa, FL

[4]Analytic Microscopy Core Facility, H. Lee Moffitt Cancer Center & Research Institute, Tampa, FL

[5]Biostatistics Core Facility, H. Lee Moffitt Cancer Center & Research Institute, Tampa, FL

[6]Breast Department, H. Lee Moffitt Cancer Center & Research Institute, Tampa, FL

[7]Division of Comparative Medicine, University of South Florida, Tampa, FL

[8]Department of Surgery, University of Florida, Gainesville, FL

[9]BIO5 Institute, University of Arizona, Tucson, AZ

Abstract

Pathologic axillary lymph node (ALN) status is an important prognostic factor for staging breast cancer. Currently, status is determined by histopathology following surgical excision of sentinel lymph node(s), which is an invasive, time consuming, costly and potentially morbid procedure. This work describes an imaging platform for the non-invasive assessment of ALN status, eliminating the need for operation in patients without nodal involvement. A targeted imaging probe (MamAb-680) was developed by conjugation of a mammaglobin-A specific monoclonal antibody to a near-infrared fluorescent dye. Using DNA and tissue microarray, mammaglobin-A was validated as a cell-surface target that is expressed in axillary lymph node positive patient samples but is not expressed in normal lymph nodes. *In vivo* selectivity was determined by intravenous injection of MamAb-680 into mice with mammaglobin-A positive and negative mammary fat pad (MFP) tumors; and by peritumoral MFP injection of the targeted imaging probe in mice with spontaneous ALN metastases. Fluorescence imaging showed that probe was only retained in positive tumors and metastases. As few as 1000 cells that endogenously express mammaglobin-A were detected in ALN indicating high sensitivity of this method. Hence, this approach has potential for translation into clinical use for the non-invasive staging of breast cancer.

Corresponding Author: David L. Morse, Department of Molecular and Functional Imaging, H. Lee Moffitt Cancer Center & Research Institute, 12902 Magnolia Drive, SRB-2, Tampa, FL 33612. Phone: 813-745-8948, Fax: 813-745-7265, david.morse@moffitt.org.

Disclosure of Potential Conflicts of Interest: No potential conflicts of interest were disclosed.

Keywords

breast cancer; imaging; lymph node metastasis; mammaglobin-A; targeted agent

Introduction

In breast cancer, the presence of disease in axillary lymph nodes is an important prognostic factor and drives treatment decision making (1, 2). Currently, most patients with breast cancer undergo axillary sentinel node biopsy for initial staging (3). Sentinel lymph nodes (SLNs) are the nodes that first receive lymph from the area of the breast harboring the tumor and are the nodes most likely to contain metastatic cells. If the SLNs are determined to be free of disease, it is accepted that all other axillary lymph nodes (ALNs) will be negative and axillary dissection can be avoided. SLN are currently identified with Tc-99m-labeled colloids (4) and/or isosulfan blue dye which is injected peri-tumorally and transiently accumulates in SLN (5, 6). Then, the sentinel nodes are removed and examined by standard pathological methods for the presence of metastasis. SLN biopsy (SLNB) can be associated with complications including seroma formation, lymphedema and sensory nerve injury (7). Furthermore, SLNB is resource intensive requiring a team with specialized training, and specialized imaging and surgical equipment (8-10).

Since there is no therapeutic value to removing uninvolved SLNs (11) development of effective, non-invasive strategies for excluding the presence of metastatic breast cancer in ALNs would represent a major advance and axillary surgery could be avoided in most early stage breast cancer patients.

Recently, several groups have investigated non-invasive imaging modalities for SLN evaluation, including single photon emission computed tomography (SPECT) (12, 13), multiphoton microscopy (14), magnetic resonance imaging (MRI)(15), optical lymphography with indocyanine green dye or multicolor quantum dots (16-19), photoacoustic tomography (PAT) using nanoparticle-based contrast agents such as carbon nanotubes (20), gold carbon nanotubes (21), gold nanocages (22), gold nanorods (23), methylene blue dye (24) and gold nanobeacons (25). However, these approaches were not targeted and thus were not able to assess SLN status. Untargeted probes distribute randomly across the SLNs with only transient and non-specific visualization of the lymphatic system. Hence, these methods only provide anatomic maps, and do not detect tumor cells present in lymph nodes.

Development of imaging agents that selectively target cancer cells with no cross-reactivity to non-tumor cells is a long-term goal for cancer imaging and could allow for the non-invasive staging of breast cancer by detection of tumor cells in ALNs. However, to date, there has been no definitive study for the development of a targeted imaging method for detection of tumor cells specifically in ALNs.

Breast cells are typically only present in the ALNs when breast cancer has spread from the primary tumor. Therefore, cell-surface marker(s) that discriminate breast epithelial cells from lymphoid cells can be used to detect metastasis (26-28). A comprehensive gene

expression analysis of breast epithelial cells versus lymphoid cells determined that mRNA encoding mammaglobin-A protein can be used to distinguish epithelial cells from lymphoid cells (29). The mammaglobin-A gene (SCGB2A2) encodes a 10-kDa glycoprotein and is a member of the epithelial secretoglobin family 2A (30, 31). Several studies have demonstrated that mammaglobin-A is exclusively expressed in breast tissue and can be used as a marker for the detection of micrometastasis in SLN [for review see (32)]. Mammaglobin-A has also been investigated as a molecular marker for targeted therapy of breast cancer (33, 34).

In the present study, we applied a high-resolution *in vivo* fluorescence imaging technique to non-invasively detect lymphatic metastasis of human breast cancer cells in a mouse model. For this purpose, a monoclonal antibody specific for binding to mammaglobin-A was conjugated to a near-infrared (NIR) fluorescent dye, (termed MamAb-680), and delivered to the lymphatic system by peritumoral injection into the mammary fat pad of nude mice, allowing imaging of mammaglobin-A expressing cells that have spread to the ALN. Thus, we have combined the specificity of a mammaglobin-A specific antibody, which binds to tumor cells, with the power of *in vivo* fluorescence imaging to demonstrate a non-invasive targeted method for detection of metastatic cells in lymph nodes. This novel approach offers a powerful targeted tool for *in vivo* studies of tumor cells within the lymphatic system, detection of tumor cells in lymph nodes, and for following the efficacy of anti-tumor therapy.

Materials and Methods

Cell culture

Human breast cancer cells, mammaglobin-A expressing ZR-75.1 (35-37) and non-expressing MDA-mb-231 (37) were grown in RPMI 1640 (Life Technologies, Gaithersburg, MD) containing 10% fetal bovine serum (Life Technologies), 0.03% L-glutamine, 100 units/mL penicillin, and 100 μg/mL streptomycin in 5% CO2 at 37 °C. Both cell lines were obtained from American Type Culture Collection (ATCC; 2007– 2009), expanded for two passages, and cryopreserved. All experiments were performed with cells of passage number less than 25. Cells were monitored by microscopy and confirmed to maintain their original morphology. Cells were tested for mycoplasma contamination by ATCC.

Generation of stably transfected ZR-75.1 cells bearing the luciferase gene

To identify the optimal concentration for selection, a range (2-10 μg/ml) of blasticidin (Invitrogen, CA) were tested on ZR-75.1 cells. ZR-75.1 cells were transfected with 5 ug of pLenti PGK Blast V5-LUC luciferase containing vector (Addgene, Cambridge, MA) using the ViraPower lentiviral expression system (Invitrogen, CA). After 2 weeks, resistant colonies appeared. Large colonies were selected and transferred to individual plates. To determine the clone with the highest expression of luciferase, warm medium containing 150 μg/ml D-luciferin potassium salt (GoldBio, MO) was prepared as substrate for the bioluminescence reaction, added to the cells and the resulting light detected by a Victor ×4 2030 multiple plate reader (PerkinElmer, CT). A clone with the brightest signal was selected and maintained in medium containing 5 ug/ml of blasticidin.

Quantitative real-time RT-PCR

Mammaglobin-A primers were designed using Gene Runner Software for Windows version 3.05: forward, 5-CTTCTTCAAGAGTTCATAGACGAC-3′ and reverse, 5′-TGCTCAGAGTTTCATCCGTTTG-3′. β-actin was used for normalization as described in our previous study (38).

DNA microarray analysis

Affymetrix expression data for the mammaglobin-A gene (SCGB2A2) in patient tissue samples were compiled from publicly available datasets. The CEL files for the tumor samples were downloaded from the Gene Expression Omnibus (GEO) database (http://www.ncbi.nlm.nih.gov/projects/geo/index.cgi), data series GSE2109. Normal tissue data were from the GEO data series GSE7307, Human Body Index. The CEL files were processed using the MAS 5.0 algorithm (Affymetrix, Santa Clara, California) and screened through a rigorous quality control panel to remove samples with a low percentage of probesets called present by the MAS 5 algorithm, indicating problems with the amplification process or poor sample quality; high scaling factors, indicating poor transcript abundance during hybridization; and poor 3′/5′ ratios, indicating RNA degradation either prior to or during processing. The remaining samples were normalized to the trimmed average of 500 in the MAS 5 algorithm before comparison of the expression values across tumors and normal samples.

Immunohistochemistry (IHC) of Tissue Mircroarray (TMA)

A TMA was constructed at the Moffitt Tissue Core containing human breast tissue samples of formalin-fixed and paraffin-embedded (FFPE) specimens. The TMA contains 50 normal breast tissue, 50 ductal carcinoma in situ, 50 invasive ductal carcinomas without metastasis, 50 invasive ductal carcinomas with metastasis and 50 lymph node with macrometastases of breast carcinoma. The TMA consists of cylindrical punches of the FFPE blocks using a Manual Tissue Arrayer (Beecher Instruments, Sun Prairie, WI).The same method was previously reported by our group for construction of a Ewing sarcoma TMA (39), except the breast TMA has only one sample per case (duplicate samples in Ewing) due to the large number of cases.

Mouse anti-mammaglobin-A mAb, 1:50, (Clone 304-1 A5, Thermo Scientific, Rockford, Illinois) was used for staining. The slides were scanned in the Moffitt Analytical Microscopy Core Facility (AMC) using an Aperio ScanScope XT digital slide scanner (Aperio, CA). The digital image of each sample was evaluated by 2 reviewers (MMB and ML).Positive staining was arbitrarily set as membranous (partial or complete) and cytoplasmic immunoreactivity in greater than or equal to 5% of tumor cells. Results were recorded as positive or negative.

Conjugation of antibody to dye

Fifteen μg human Mammaglobin-A specific mouse mAb (Zeta Corp., Sierra Madre, CA) was incubated with 10 μg VivoTag-S 680 (VisEn Medical, Bedford, MA) and purified with a Sephadex G25 column (Roche, Indianapolis, IN). Protein (A280) and dye (A680) absorbance was determined using an ND-1000 spectrophotometer (NanoDrop, Wilmington,

DE) and used to confirm the number of fluorophore molecules conjugated to each antibody molecule.

Microscopic studies

Cells and tissues from positive and negative xenograft tumors were fixed with cold methanol:acetone and incubated with 1 μg/μl MamAb-680 and 5.0 μg/mL of WGA (Invitrogen, Carlsbad, California) for 30 min. After three washes with PBS, coverslips were mounted using mounting medium with DAPI, 4′,6-diamidino-2-phenylindole (Vector Laboratories, Inc., Burlingame, CA). Micrographs were acquired at 200 Hz in the Moffitt Analytical Microscopy Core using a Leica DMI6000 inverted microscope and TCS SP5 tandem confocal scanner, through a 63×/1.40NA Plan Apochromat oil immersion objective lens (Leica Microsystems, Germany) with dual photomultiplier tube detectors. Lasers, 405 diode (DAPI/Lysotracker Blue), 488 tunable argon (Green dye) and 543 diode (Rhodamine), were applied to excite the samples and a tunable emissions filter was used to eliminate crosstalk between fluorochromes. LAS AF software version 2.1.0 (Leica Microsystems, Germany) was used to acquire and save the images using 0% compression of the original files.

To determine cell surface localization, cells were incubated with 1 μg/μl mammaglobin antibody conjugated to dye and 5.0 μg/mL of WGA at 4°C for 10 min, washed 3 times with PBS, fixed with cold methanol:acetone, air dried for 20 min, mounted and viewed as described above.

Tumor xenograft studies

All procedures were carried out in compliance with the Guide for the Care and Use of laboratory Animal Resources (1996), National Research Council, and approved by the Institutional Animal Care and Use Committee, University of South Florida.

Female *nu/nu* mice 6-8 weeks old (Harlan Sprague Dawley, Inc., Indianapolis, IN) were implanted subcutaneously (s.c.) with a 60 d estrogen-release pellet containing 0.72 mg of estradiol (Innovative Research of America, Sarasota, FL) under 3 to 4% isoflurane anesthesia. Two days after implantation, 5×10^6 ZR-75.1 and MDA-mb-231 cells are implanted in the right and left mammary fat pad (MFP) respectively. Tumor volume was determined with calipers using the formula: volume = (length × width^2)/2. Once tumors reached 500-800 mm^3, 50 μg MamAb-680, in 100 μL sterile saline, was injected into the tail vein. In vivo fluorescence images were acquired using an IVIS-200 small animal imaging system (Caliper LifeSciences, Hopkinton, MA) using a 615-665 nm excitation filter and a 695-770 nm emission filter. The excitation maxima of the unconjugated VivoTag-S™ 680 dye is 673 ±5 nm and the emission maxima is 691 ±5 according to manufacturer. Living Image 3.2 Software was used to draw regions of interest (ROIs) over the tumors to determine the mean tumor surface radiance (photons/sec/steradian/cm^2). Autofluorescence background was subtracted by determining the mean tumor fluorescence signal prior to injection.

Pharmacodynamics studies were performed by imaging at various time points. For biodistribution studies, mice were imaged and euthanized at 24 h post-injection, tissues excised, rinsed with PBS, blotted dry, and then imaged ex vivo in the IVIS-200. A center slice cut from the tumor was imaged and the remaining halves were formalin fixed and fresh frozen, respectively, as described below. Mean surface radiance was determined for each tumor and organ. Autofluorescence background was subtracted using measurements from comparable tissues from an untreated animal.

Orthotopic implantation of cells into ALN

Female *nu/nu* mice 6-8 weeks old were implanted with an estrogen-release pellet (see above). Two days after implantation, luciferase expressing ZR-75.1 cells were injected into the axillary lymph node using ultrasound image guidance: Mice were anesthetized with 3-4% isoflurane using a nose-cone manifold and restrained on the stage of a VEVO 770 high-resolution small animal ultrasound imaging system (VisualSonics, Toronto, Canada) using tape; ultrasound gel was applied to the area over the axillary node; the 40MHz ultrasound probe was placed in the probe guide and the node located by mechanically adjusting the probe guide to resolve the nodes; a 1 cc syringe with a 29 gauge needle was loaded with 100 to 100,000 cells in a 20 μL volume of 1:1 matrigel and sterile PBS and positioned in the needle guide so that the end of the needle could be moved into the node and cells injected. Ultrasound images were acquired at the time of each injection. Four h after injection of cells, animals were anesthetized and 300 μl of 15 mg/ml D-luciferin potassium salt (GoldBio, MO) was introduced via intraperitoneal (i.p.) injection. Five min after the injection, a bioluminescence image was acquired using standard bioluminescence settings on the IVIS-200. Twenty-four h after injection of cells, MamAb-680 was injected into the mammary fat pad proximal to axillary nodes, and fluorescence imaging was performed using the IVIS-200 as described above for pharmacodynamics and biodistribution studies.

Statistics—Data are represented as mean ± s.d. and the t-test was used to determine significance.

Results

Mammaglobin-A expression in patient tissue samples

Several studies have demonstrated high expression of mammaglobin-A in breast cancer [for review see (32)]. For further confirmation and to characterize mRNA expression in patient tissue samples, including lymph node metastases and normal tissues, we analyzed publicly available DNA microarray data sets. Mammaglobin-A mRNA was highly and generally expressed in breast tumors, breast cancer lymph node metastases and in normal breast (Fig. 1). A high percentage (83%) of lymph node metastases expressed mammoglobin-A. In contrast, mammaglobin-A was not expressed in normal lymph nodes. Also, other organs involved in toxicity or drug clearance, i.e. liver, kidney, heart, lung and spleen did not express mammaglobin-A mRNA.

To determine mammaglobin-A protein expression in patient samples, immunohistochemistry (IHC) was performed on a breast cancer tissue microarray containing 250 samples. Positive staining was observed in the ductal epithelium of 63% of normal breast tissues (Supplementary Fig. S1A, B), 80% DCIS, 53% invasive ductal carcinoma without metastasis, 43% invasive ductal carcinoma with metastasis and 45% lymph node with macrometastasis of breast cancer (Supplementary Fig. S1C, D).

ZR-75.1 breast cancer cells express mammaglobin-A

ZR-75.1 breast cancer cells endogenously express mammaglobin-A (35-37) and MDA-mb-231 cells do not (37). To confirm this, mammaglobin-A mRNA expression was quantified by qRT-PCR in ZR-75.1 cells, but MDA-mb-231 cells did not express. Western blot and immunocytochemistry (ICC) also confirmed protein expression (Supplementary Fig. S2A, B).

Antibody and MamAb-680 characterization

Three different mammaglobin-A monoclonal antibodies were evaluated for sensitivity and specificity by Western blot and ICC (Supplementary Fig. S2C, D). From these studies a specific mAb (Zeta Corp.) was selected for conjugation to near-infrared dye (VivoTag-S 680). To evaluate the antibody-dye conjugation and to verify that MamAb-680 retained binding specificity, ICC using the dye-labeled primary antibody was performed on the endogenously expressing ZR-75.1 cells, MDA-mb-231 cells engineered to express mammaglobin-A (Supplementary Fig. S2E) and the non-expressing MDA-mb-231 cells. MamAb-680 bound only to expressing cells (Fig. 2A). Hence, the conjugated agent retained specificity for mammaglobin-A protein.

Mammaglobin-A is expressed on the cell-surface

Zuo et al., recently reported that mammaglobin-A is directly associated with the surface of breast cancer cells (34). As described above, permeabilized fixed cells were used for ICC. To verify cell-surface expression, ZR-75.1 cells were incubated with MamAb-680 at 4°C, and agent was observed at the cell surface co-localized with agglutinin dye (Fig. 2B). Western blots of membrane protein extracts of mammaglobin-A positive cells stained positive for mammaglobin-A protein (Supplementary Fig. S2F).

MamAb-680 selectively accumulates in positive tumors

To determine the specificity of MamAb-680 targeting *in vivo*, ZR-75.1 and MDA-mb-231 cells were implanted in the right and left mammary fat pads (MFP) of female nude mice. After tumor growth to approximately 500-800 mm^3 in volume, MamAb-680 was intravenously (i.v.) injected. As shown in Fig. 3A, ZR-75.1 tumors retained higher levels of the agent signal compared to MDA-mb-231. Signal in the positive tumor was quantified as having an 8.6 ± 0.8 s.d. ($n=4$, $p<0.001$) fold enhancement relative to the negative tumor, 24 h post-injection. As a second test of agent specificity, a blocking experiment was performed where ZR-75.1 tumor-bearing mice were pre-injected with an excess (250 μg) of unlabeled mammaglobin-A antibody, followed by injection of 50 μg of MamAb-680. The unlabeled mammaglobin antibody effectively reduced the fluorescence signal 6.6 fold in the tumor

relative to the previous experiment without addition of blocking antibody (Fig. 3B). These results demonstrate the *in vivo* targeting specificity of MamAb-680.

To confirm the presence of mammaglobin-A protein *in vivo*, sections from flash-frozen tumors were stained with MamAb-680, a nuclear stain, (DAPI), and a cell-surface/ cytoplasmic stain, wheat germ agglutinin (WGA), and analyzed using confocal microscopy (Fig. 2C). Mammaglobin-A staining was only observed in tumors from the positively expressing cell line but not in the negative line. Ex-vivo images of the corresponding center sections of the tumors confirmed MamAb-680 localization to the positive tumor relative to the negative tumor (Fig 2D).

Pharmacodynamics and biodistribution of MamAb-680

To assess the pharmacodynamics of tumor uptake and clearance, MamAb-680 was intravenously (i.v.) injected and images acquired at intervals from 5 min to 12 d post injection. Fluorescence signal increased for 24 h and then slowly decreased at later time-points (Fig. 4A). Elevation of fluorescence in the positive tumor relative to the negative tumor was detected from 4 h to 10 days after injection.

For biodistribution studies, mammaglobin-positive and -negative tumor-bearing mice were i.v. injected with MamAb-680 and 24 h later, tumors and organs were removed and imaged *ex vivo*. Fig. 4B demonstrates that fluorescence was present in the positive tumor but has largely cleared from the negative tumor and other organs.

MamAb-680 detects tumor cells in axillary lymph nodes

Previously, it was not reported that ZR-75.1 cells form ALN metastases. To determine this, 5×10^6 ZR-75.1/Luc cells were implanted into the right MFP of estrogen-pelleted mice. Three weeks after implantation, tumors were surgically removed. Two weeks later, the tumor had regrown and bioluminescence imaging showed metastasis to the ALN (Fig. 3C). Hence, ZR-75.1 cells are a suitable model for ER+ breast cancer lymph node metastasis.

To investigate whether MamAb-680 can be delivered through the lymphatics and are selectively retained in ALN bearing mammaglobin-A expressing metastases, agent was injected peritumorally into the MFP. At 24 h post-injection, a strong fluorescence signal was obtained from the area of the ALN (Fig. 3D), which co-localized with the bioluminescence image of the luciferase expressing metastases (3C). After imaging, the metastases were removed and determined to be composed of cancer cells by H & E staining and pathological examination (3E).

Agent selectivity for positive lymph nodes was also determined using an orthotopic model of lymph node metastasis. ZR-75.1/luc cells were directly injected into the ALN using ultrasound image guidance (Fig. 5A) and were detected by bioluminescence (Fig. 5B). MamAb-680 was delivered by MFP injection and was observed to have traversed to the lymph node within 4 h (Fig. 5C). Fluorescence signal was retained in lymph nodes implanted with mammaglobin-A positive cells (Fig. 5D) long after clearance from the MFP and negative lymph nodes. Positive lymph nodes were resolved as early as 4 h and were detected up to at least 7 days post-injection. Our results show that *in vivo* lymphatic imaging

using MamAb-680 provided a specific and durable signal in mammaglobin-A expressing lymph node metastases.

As a control, one million MDA-mb-231 cells were injected into the ALN as a mammaglobin-A negative control using the same method and amounts described above, then MamAb-680 was injected into the MFP and imaged (Fig. 5E). A corresponding post-injection bioluminescence image confirmed the presence of cells in the ALN (supplementary Fig. S3A). Minimal signal was detected in the draining lymphatics at 4 h post-injection and no signal was observed at 24 h (Fig. 5F). At 48 h, agent was cleared from the animal. Hence, the fluorescence signal is specific for mammaglobin-A expressing cells in the ALN. As an additional control, ALN were sham-injected with PBS and matrigel (no cells). In this case, the same result was observed as seen for the mammaglobin-A negative cells above (Supplementary Fig. S3D & E).

To determine the sensitivity of the agent, a range in number of ZR-75.1/luc (1000 to 1 million) were injected into ALN via ultrasound guidance. For confirmation of successful cell implantation, bioluminescence images were acquired and as few as 1,000 cells were detected (Fig. 6A). Four hours after cell injection, MamAb-680 was injected into mammary fat pad proximal to the ALN and fluorescence images were acquired 24 h after injection (Fig. 6B). Bioluminescent and fluorescent signals were quantified by drawing a region-of-interest (ROI) encompassing the tumor cells in the ALN. Signal intensity decreased with cell number and at least 1,000 cells were detectable above background (Fig. 6B and supplementary Figs. S4A, B).

Discussion

To the best of our knowledge, this is the first report of the development of a targeted method for non-invasive detection of breast cancer cells in lymph nodes. Using a novel molecular imaging agent (MamAb-680) and a mouse model, we have demonstrated the non-invasive detection of breast cancer lymph node metastases bearing a specific marker, mammaglobin-A. The agent was generated by conjugating a NIR fluorescent dye to a monoclonal antibody that is determined to be highly specific for binding to mammaglobin-A.

Since breast cells are found in ALNs primarily in the case of regional metastasis, markers generally specific for breast cells can be used for detection of nodal disease. Here, we have used mammaglobin-A which is expressed in a percentage of all types of breast cancer, including lymph node positive samples and its expression in normal tissues is restricted to the intraductal epithelia of the mammary gland. Mammaglobin-A mRNA was not detected in any other tissue including normal lymph nodes. Gene expression profiling of breast epithelial cells versus lymphoid cells has shown that mammaglobin-A is a robust mRNA for distinguishing epithelial cells from lymphoid cells (29), which is in agreement with the results reported herein.

IHC staining for mammaglobin-A in a breast tissue microarray revealed that 45.2% of lymph nodes with macrometastases were positive for mammaglobin-A. This was lower than frequencies (48% to 84%) reported previously by several groups using different antibodies

(30, 40-43). Although mammaglobin-A is a member of the secretoglobin family and is generally considered to be secreted, our results showed that mammaglobin protein is associated with the surface of breast cancer cells, which is in agreement with Zue et al. (34). Hence, the membrane-associated mammaglobin-A can be utilized as a molecular marker for targeting imaging agents to breast cancer metastases.

We have reported for the first time that ZR-75.1 breast cancer cells form spontaneous metastases to ALNs in nude mice. MDA-mb-231, an invasive breast cancer cell line, is widely used in breast cancer lymph node metastasis studies, and these cells require at least 6-8 weeks after implantation to form detectable metastases (44). However, ZR-75.1 cells were detected in the ALN as early as five weeks after xenografting the cells into the mammary fat pad. Hence, ZR-75.1 cells are a robust model for breast cancer lymph node metastasis studies.

In vivo fluorescence imaging has emerged as an excellent method for the non-invasive imaging of tissues with high spatial resolution. Optical imaging allows for the real-time visualization of specific molecular markers, in disease, prognosis, staging and therapy monitoring (45). Our *in vit*ro and *in vivo* studies demonstrated a superb high selectivity of the agent, where 8.6 ± 0.8 fold enhancement of positive tumor was observed relative to the negative tumor. Although mammaglobin-A is expressed in normal breast, its distribution is limited to the epithelia, which is not accessible to the agent, which is injected into the parenchyma.

To determine the sensitivity of our method, we developed a novel orthotopic xenograft model for lymph node metastasis, where precise numbers of cells were injected into the ALNs using ultrasound image guidance. As few as 1,000 cells were quantitatively detected in the ALN. Hence, our method may overcome the problem of interobserver variation in classification of metastatic disease as macrometastasis (> 2mm), micrometastasis (between 0.2 and 2 mm) or individual tumor cells or groups of cells (ITCs, <0.2 mm)(46, 47). One-thousand cells represent a volume of approximately 1 nL, which is well below the size of a micrometastasis. Additionally, detection of ITCs in prenodal lymph before colonization in the lymph node was shown to be possible.

In the future, the level of detection may be improved by using a fluorescent dye with longer excitation and emission wavelengths, e.g. 800-900 nm; or through the use of another imaging modality, such as detection of positron or single photon emission, MRI, nanoparticle or NIR dye-based photoacoustic tomography, or by using a more sophisticated fluorescence imaging system, e.g. with spectral unmixing or fluorescence lifetime capability, compared to the surface radiance (planar) imaging system used in this study. Additionally, our fluorescent targeted agents could be used intraoperatively for image guided surgery to remove involved nodes and leave uninvolved nodes (48). To add therapeutic capability, targeted gold nanoparticles could be used for both non-invasive imaging via photoacoustic tomography (PAT) as well as delivering therapy through photothermal ablation (49). The targeted nanoparticles could thus be heated using laser light to destroy cells and tissue adhered to the agent, i.e. “molecular surgery.” Regional control in the lymph nodes after targeting metastatic cancer could eliminate the need for surgery to

remove the diseased nodes and therefore reduce significant complications, e.g. lymphedema. Furthermore, cancer imaging of metastatic lymph nodes could provide response assessment to traditional therapeutic options such as cytotoxic or molecular-targeted chemotherapy, and axillary radiotherapy.

According to the pharmacokinetics study, the optimal time for imaging was 24 h after administration of the agent, at which time the agent had reached peak levels in the involved node and was cleared from surrounding tissues. However, positive lymph nodes were detected as early as 4 h. Since this antibody-based agent is relatively large compared to synthetic peptide-based ligands, the time required for SLN uptake and clearance could be improved by the development of a smaller mammaglobin-A specific ligands or peptibodies.

According to our IHC data, mammaglobin is expressed in 45.2% of lymph node positive samples. Therefore, agents specific for additional markers expressed in lymph node metastases will be required, in combination with the mammaglobin-A targeting probe, in order detect all breast cancer lymph node metastses. For example, it has been reported that the combination of mammaglobin-A and cytokeratin-19 (CK19) is an optimal molecular marker set for the detection of clinically actionable metastases in breast lymph nodes with 90% sensitivity and 94% specificity (29). Unfortunately CK19 is not a cell-surface marker. Through gene expression profiling and IHC validation of protein expression in patient tissue samples, we are in the process of identifying additional cell-surface markers that in combination with mammaglobin-A will detect all breast cancer lymph node metastases.

In summary, our results demonstrate that the breast cancer targeted agent, MamAb-680 can be used for the non-invasive, *in vivo* detection of cancerous cells in mouse axillary lymph nodes with high resolution and specificity. This targeted imaging strategy has potential for future translation into the clinic for SLN assessment and intraoperative surgical guidance. In the future, this agent may be improved by development of small peptide-based ligands and through the possible attachment to nanoparticles for delivery of imaging contrast and therapy.

Supplementary Material

Refer to Web version on PubMed Central for supplementary material.

Acknowledgments

The authors thank the staff of the Moffitt Small Animal Modeling and Imaging Shared Resource, Microarray Core, Tissue Core, and Analytic Micorscopy Core for their technical support.

Grant Support: University of Florida/Moffitt Cancer Center Collaborative Initiative Grant, UF 69-15540-01-01, University of Florida, Gainesville, FL.

References

1. Stacker SA, Achen MG, Jussila L, Baldwin ME, Alitalo K. Lymphangiogenesis and cancer metastasis. Nat Rev Cancer. 2002; 2:573–83. [PubMed: 12154350]
2. Tafreshi NK, Kumar V, Morse DL, Gatenby RA. Molecular and functional imaging of breast cancer. Cancer Control. 17:143–55. [PubMed: 20664511]

3. Oncology. Vol. 5. Williston Park: 1991. NIH Consensus Development Conference statement on the treatment of early-stage breast cancer; p. 120-4.
4. Mariani G, Erba P, Villa G, et al. Lymphoscintigraphic and intraoperative detection of the sentinel lymph node in breast cancer patients: the nuclear medicine perspective. J Surg Oncol. 2004; 85:112–22. [PubMed: 14991882]
5. Borgstein PJ, Meijer S, Pijpers R. Intradermal blue dye to identify sentinel lymph-node in breast cancer. Lancet. 1997; 349:1668–9. [PubMed: 9186389]
6. Maza S, Valencia R, Geworski L, et al. Peritumoural versus subareolar administration of technetium-99m nanocolloid for sentinel lymph node detection in breast cancer: preliminary results of a prospective intra-individual comparative study. Eur J Nucl Med Mol Imaging. 2003; 30:651–6. [PubMed: 12612811]
7. Purushotham AD, Upponi S, Klevesath MB, et al. Morbidity after sentinel lymph node biopsy in primary breast cancer: results from a randomized controlled trial. J Clin Oncol. 2005; 23:4312–21. [PubMed: 15994144]
8. Krag D, Weaver D, Ashikaga T, et al. The sentinel node in breast cancer--a multicenter validation study. N Engl J Med. 1998; 339:941–6. [PubMed: 9753708]
9. McMasters KM, Tuttle TM, Carlson DJ, et al. Sentinel lymph node biopsy for breast cancer: a suitable alternative to routine axillary dissection in multi-institutional practice when optimal technique is used. J Clin Oncol. 2000; 18:2560–6. [PubMed: 10893287]
10. Ung OA. Australasian experience and trials in sentinel lymph node biopsy: the RACS SNAC trial. Asian J Surg. 2004; 27:284–90. [PubMed: 15564180]
11. Krag DN, Anderson SJ, Julian TB, et al. Primary outcome results of NSABP-32, a randomized phase III trial to compare sentinel node resection (SNR) to conventional axillary dissection (AD) in clinically node-negative breast cancer patients. Journal of clinical oncology. 2010; 28:18s.
12. Ibusuki M, Yamamoto Y, Kawasoe T, et al. Potential advantage of preoperative three-dimensional mapping of sentinel nodes in breast cancer by a hybrid single photon emission CT (SPECT)/CT system. Surg Oncol. 2009
13. van der Ploeg IM, Valdes Olmos RA, Kroon BB, Nieweg OE. The Hybrid SPECT/CT as an additional lymphatic mapping tool in patients with breast cancer. World J Surg. 2008; 32:1930–4. [PubMed: 18478289]
14. Makale M, McElroy M, O'Brien P, et al. Extended-working-distance multiphoton micromanipulation microscope for deep-penetration imaging in live mice and tissue. J Biomed Opt. 2009; 14:024032. [PubMed: 19405761]
15. Mortellaro VE, Marshall J, Singer L, et al. Magnetic resonance imaging for axillary staging in patients with breast cancer. J Magn Reson Imaging. 2009; 30:309–12. [PubMed: 19466713]
16. Kim S, Lim YT, Soltesz EG, et al. Near-infrared fluorescent type II quantum dots for sentinel lymph node mapping. Nat Biotechnol. 2004; 22:93–7. [PubMed: 14661026]
17. Kobayashi H, Hama Y, Koyama Y, et al. Simultaneous multicolor imaging of five different lymphatic basins using quantum dots. Nano Lett. 2007; 7:1711–6. [PubMed: 17530812]
18. Kobayashi H, Ogawa M, Kosaka N, Choyke PL, Urano Y. Multicolor imaging of lymphatic function with two nanomaterials: quantum dot-labeled cancer cells and dendrimer-based optical agents. Nanomedicine (Lond). 2009; 4:411–9. [PubMed: 19505244]
19. Ogata F, Azuma R, Kikuchi M, Koshima I, Morimoto Y. Novel lymphography using indocyanine green dye for near-infrared fluorescence labeling. Ann Plast Surg. 2007; 58:652–5. [PubMed: 17522489]
20. Pramanik M, Song KH, Swierczewska M, Green D, Sitharaman B, Wang LV. In vivo carbon nanotube-enhanced non-invasive photoacoustic mapping of the sentinel lymph node. Phys Med Biol. 2009; 54:3291–301. [PubMed: 19430111]
21. Kim JW, Galanzha EI, Shashkov EV, Moon HM, Zharov VP. Golden carbon nanotubes as multimodal photoacoustic and photothermal high-contrast molecular agents. Nat Nanotechnol. 2009; 4:688–94. [PubMed: 19809462]
22. Song KH, Kim C, Cobley CM, Xia Y, Wang LV. Near-infrared gold nanocages as a new class of tracers for photoacoustic sentinel lymph node mapping on a rat model. Nano Lett. 2009; 9:183–8. [PubMed: 19072058]

23. Song KH, Kim C, Maslov K, Wang LV. Noninvasive in vivo spectroscopic nanorod-contrast photoacoustic mapping of sentinel lymph nodes. Eur J Radiol. 2009; 70:227–31. [PubMed: 19269762]
24. Song KH, Stein EW, Margenthaler JA, Wang LV. Noninvasive photoacoustic identification of sentinel lymph nodes containing methylene blue in vivo in a rat model. J Biomed Opt. 2008; 13:054033. [PubMed: 19021413]
25. Pan D, Pramanik M, Senpan A, et al. Near infrared photoacoustic detection of sentinel lymph nodes with gold nanobeacons. Biomaterials. 2010; 31:4088–93. [PubMed: 20172607]
26. Abdul-Rasool S, Kidson SH, Panieri E, Dent D, Pillay K, Hanekom GS. An evaluation of molecular markers for improved detection of breast cancer metastases in sentinel nodes. J Clin Pathol. 2006; 59:289–97. [PubMed: 16505281]
27. Douglas-Jones AG, Woods V. Molecular assessment of sentinel lymph node in breast cancer management. Histopathology. 2009; 55:107–13. [PubMed: 19469912]
28. Inokuchi M, Ninomiya I, Tsugawa K, Terada I, Miwa K. Quantitative evaluation of metastases in axillary lymph nodes of breast cancer. Br J Cancer. 2003; 89:1750–6. [PubMed: 14583780]
29. Backus J, Laughlin T, Wang Y, et al. Identification and characterization of optimal gene expression markers for detection of breast cancer metastasis. J Mol Diagn. 2005; 7:327–36. [PubMed: 16049304]
30. Watson MA, Dintzis S, Darrow CM, et al. Mammaglobin expression in primary, metastatic, and occult breast cancer. Cancer Res. 1999; 59:3028–31. [PubMed: 10397237]
31. Watson MA, Fleming TP. Mammaglobin, a mammary-specific member of the uteroglobin gene family, is overexpressed in human breast cancer. Cancer Res. 1996; 56:860–5. [PubMed: 8631025]
32. Zehentner BK, Carter D. Mammaglobin: a candidate diagnostic marker for breast cancer. Clin Biochem. 2004; 37:249–57. [PubMed: 15003725]
33. Goedegebuure PS, Watson MA, Viehl CT, Fleming TP. Mammaglobin-based strategies for treatment of breast cancer. Curr Cancer Drug Targets. 2004; 4:531–42. [PubMed: 15462037]
34. Zuo L, Li L, Wang Q, Fleming TP, You S. Mammaglobin as a potential molecular target for breast cancer drug delivery. Cancer Cell Int. 2009; 9:8. [PubMed: 19309500]
35. Guan XF, Hamedani MK, Adeyinka A, et al. Relationship between mammaglobin expression and estrogen receptor status in breast tumors. Endocrine. 2003; 21:245–50. [PubMed: 14515009]
36. Min CJ, Tafra L, Verbanac KM. Identification of superior markers for polymerase chain reaction detection of breast cancer metastases in sentinel lymph nodes. Cancer Res. 1998; 58:4581–4. [PubMed: 9788605]
37. Zafrakas M, Petschke B, Donner A, et al. Expression analysis of mammaglobin A (SCGB2A2) and lipophilin B (SCGB1D2) in more than 300 human tumors and matching normal tissues reveals their co-expression in gynecologic malignancies. BMC Cancer. 2006; 6:88. [PubMed: 16603086]
38. Morse DL, Carroll D, Weberg L, Borgstrom MC, Ranger-Moore J, Gillies RJ. Determining suitable internal standards for mRNA quantification of increasing cancer progression in human breast cells by real-time reverse transcriptase polymerase chain reaction. Anal Biochem. 2005; 342:69–77. [PubMed: 15958182]
39. Schlauder SM, Steffensen TS, Morgan M, et al. Assessment of muscarinic and nicotinic acetylcholine receptor expression in primitive neuroectodermal tumor/ewing family of tumor and desmoplastic small round cell tumor: an immunohistochemical and Western blot study of tissue microarray and cell lines. Fetal Pediatr Pathol. 2008; 27:83–97. [PubMed: 18568996]
40. Bhargava R, Beriwal S, Dabbs DJ. Mammaglobin vs GCDFP-15: an immunohistologic validation survey for sensitivity and specificity. Am J Clin Pathol. 2007; 127:103–13. [PubMed: 17145637]
41. Han JH, Kang Y, Shin HC, et al. Mammaglobin expression in lymph nodes is an important marker of metastatic breast carcinoma. Arch Pathol Lab Med. 2003; 127:1330–4. [PubMed: 14521461]
42. Sasaki E, Tsunoda N, Hatanaka Y, Mori N, Iwata H, Yatabe Y. Breast-specific expression of MGB1/mammaglobin: an examination of 480 tumors from various organs and clinicopathological analysis of MGB1-positive breast cancers. Mod Pathol. 2007; 20:208–14. [PubMed: 17192791]
43. Wang Z, Spaulding B, Sienko A, et al. Mammaglobin, a valuable diagnostic marker for metastatic breast carcinoma. Int J Clin Exp Pathol. 2009; 2:384–9. [PubMed: 19158935]

44. Price JE, Polyzos A, Zhang RD, Daniels LM. Tumorigenicity and metastasis of human breast carcinoma cell lines in nude mice. Cancer Res. 1990; 50:717–21. [PubMed: 2297709]

45. Massoud TF, Gambhir SS. Molecular imaging in living subjects: seeing fundamental biological processes in a new light. Genes Dev. 2003; 17:545–80. [PubMed: 12629038]

46. Greene, FL. AJCC cancer staging handbook-TNM classification of malignant tumors. New York: Springer; 2002.

47. Sobin, LH. UICC TNM classification of malignant tumors. Chichester: John Wiley & Sons; 2002.

48. Troyan SL, Kianzad V, Gibbs-Strauss SL, et al. The FLARE intraoperative near-infrared fluorescence imaging system: a first-in-human clinical trial in breast cancer sentinel lymph node mapping. Ann Surg Oncol. 2009; 16:2943–52. [PubMed: 19582506]

49. Sharma P, Brown SC, Bengtsson N, et al. Gold-Speckled Multimodal Nanoparticles for Noninvasive Bioimaging. Chem Mater. 2008; 20:6087–94. [PubMed: 19466201]

Abbreviations

MamAb-680	Mammaglobin monoclonal antibody conjugated to VivoTag-S 680
Mam	Mammaglobin

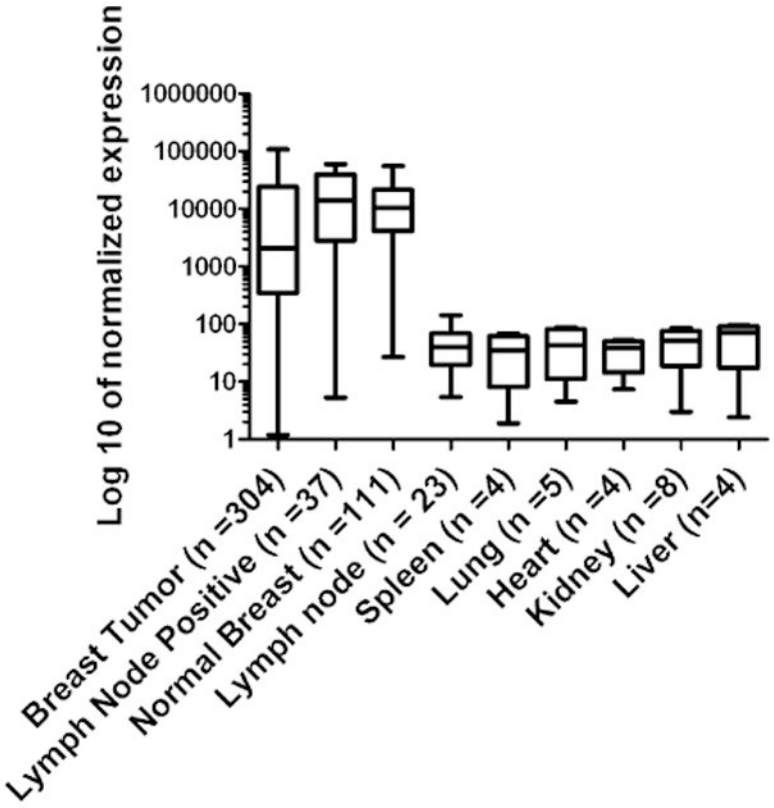

Figure 1.

DNA microarray expression profile of Mammaglobin-A in breast cancer and normal tissues. Data are represented as mean ± s.d. Note the Log 10 scale.

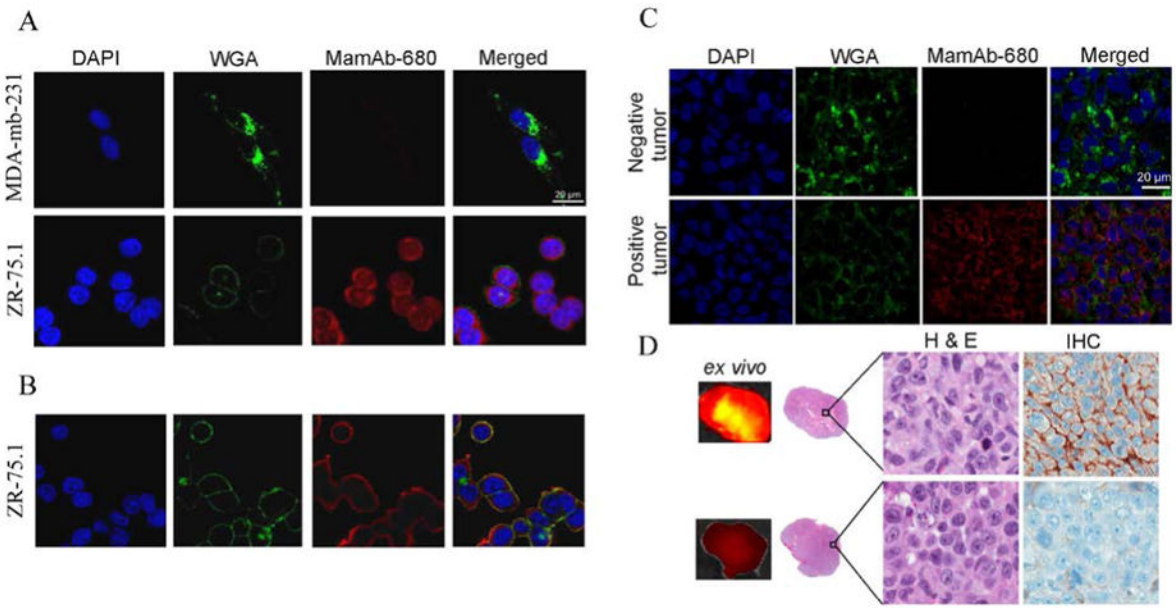

Figure 2.

Specific binding of MamAb-680 to mammaglobin-A expressing cells and tumor sections and *ex vivo* analysis of negative and positive tumors. Confocal micrographs of cells incubated with the nuclear marker DAPI (blue), the plasma- and cytoplasmic-membrane marker, WGA (green) and MamAb-680 (red). (A) Agent (red) is not present in non-expressing MDA-mb-231 cells, but is present in mammaglobin-A expressing ZR-75.1 cells. (B) Cell surface staining of ZR.75.1 cells. Merged image shows colocalization of agent (red) with membrane marker (green) indicating accumulation of agent on the cell-surface. (C) Confocal microscopy of negative and positive tumor sections. (D) *Ex vivo* images of tumor with corresponding histology and mammaglobin-A IHC staining of positive and negative tumors.

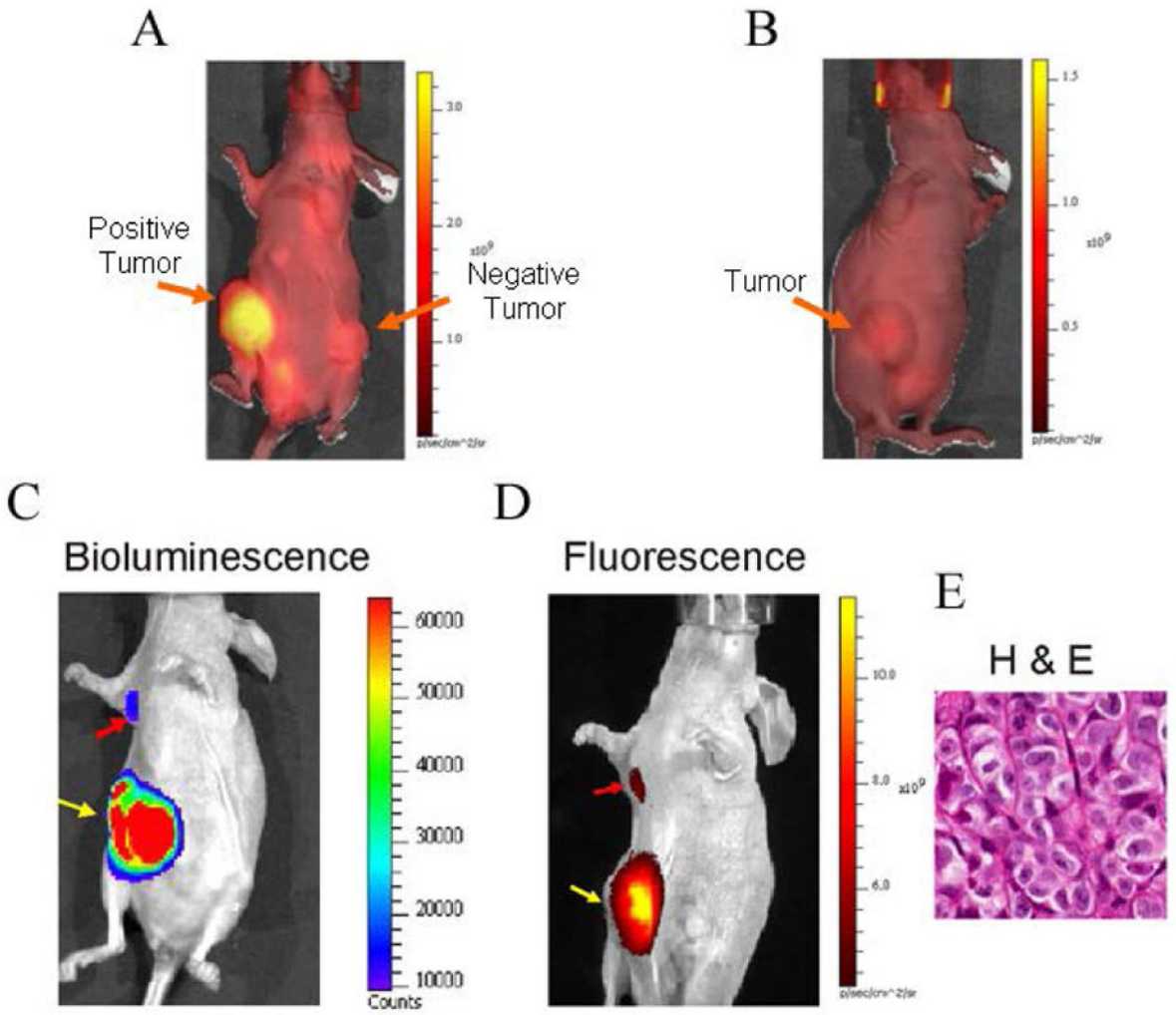

Figure 3.

In vivo selectivity and representative *in vivo* images of spontaneous metastasis into the axillary lymph node by luciferase expressing ZR-75.1 human breast cancer cells. (A) *In vivo* fluorescence image of mouse bearing positive (ZR-75.1) and negative (MDA-mb-231) xenograft tumors, 24 h post injection of agent. Autofluorescence background signal is observed throughout the animal. Note the bright signal in the positive tumor and that agent has cleared from the entire mouse, including the negative tumor at this time-point. (B) Fluorescence image of a ZR-75.1 MFP tumor bearing mouse that was preinjected with 250 μg unlabeled mammaglobin-A monoclonal antibody, and 4 h later followed by injection of 50 μg MamAb-680. The image was acquired 24 h after injection with labeled probe. (C) Bioluminescence image of luciferase activity in the primary tumor (yellow arrow) and axillary lymph node metastasis (red arrow). (D) After peritumoral injection (24 h) of MamAb-680, the same mouse was imaged for fluorescence, and signal was observed to emit from the mammaglobin-A expressing (ZR-75.1) axillary lymph node metastasis (red arrow) and primary tumor (yellow arrow), following clearance of MamAb-680 from the MFP. (E) H & E staining of the ALN metastasis from the same mouse. It was noted that the shape of

the metastasis matched the elongated shape observed in both the bioluminescence and fluorescence images.

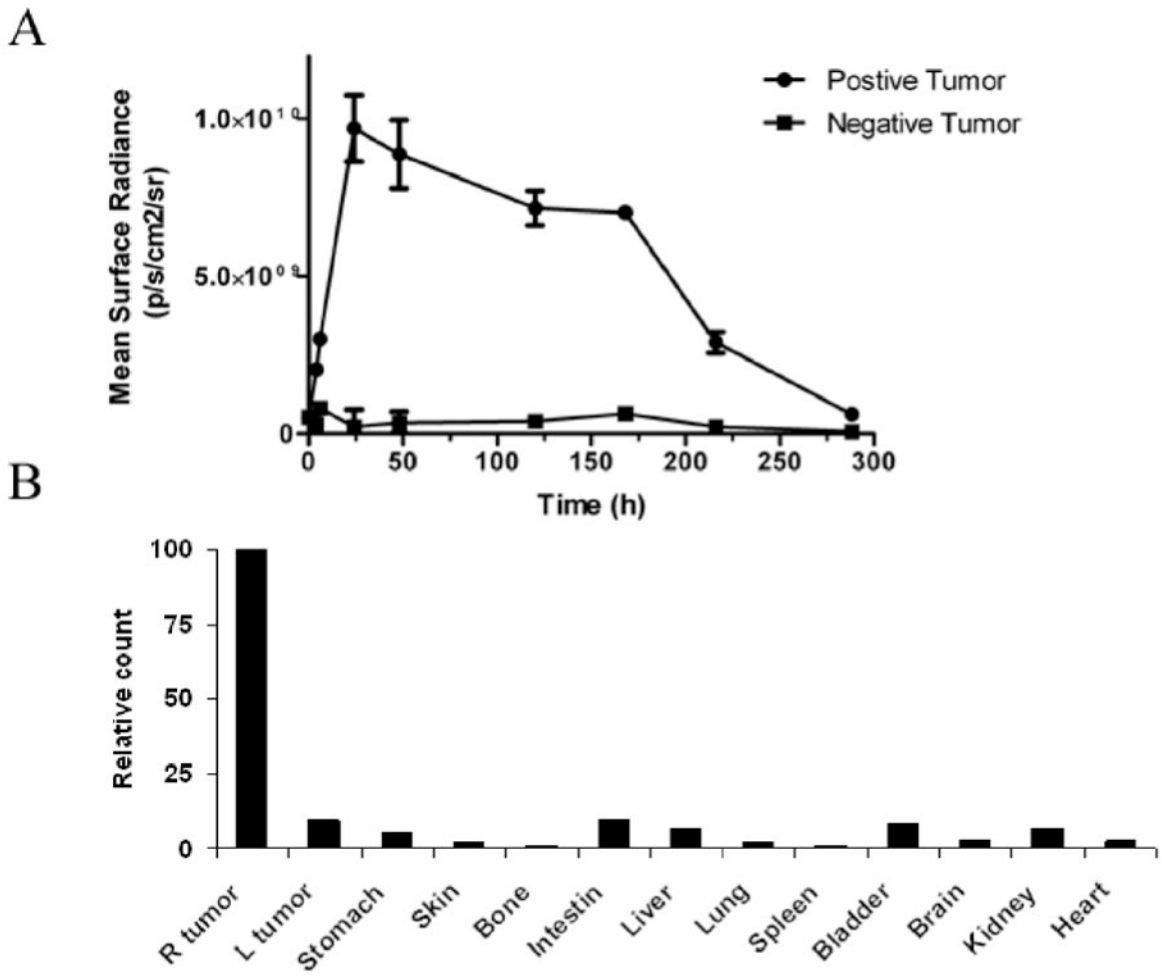

Figure 4.

Pharmacodynamics and biodistribution of MamAb-680. (A) Pharmacodynamics of agent in positive and negative tumors. Note the peak signal in the positive tumor at 24 h and that agent is nearly cleared by 12 days post-injection. Data represent mean ± s.d. (B) Biodistribution of agent in the tumors and organs 24 h post-injection shows predominant positive tumor localization. The values were normalized as percentage of the highest signal.

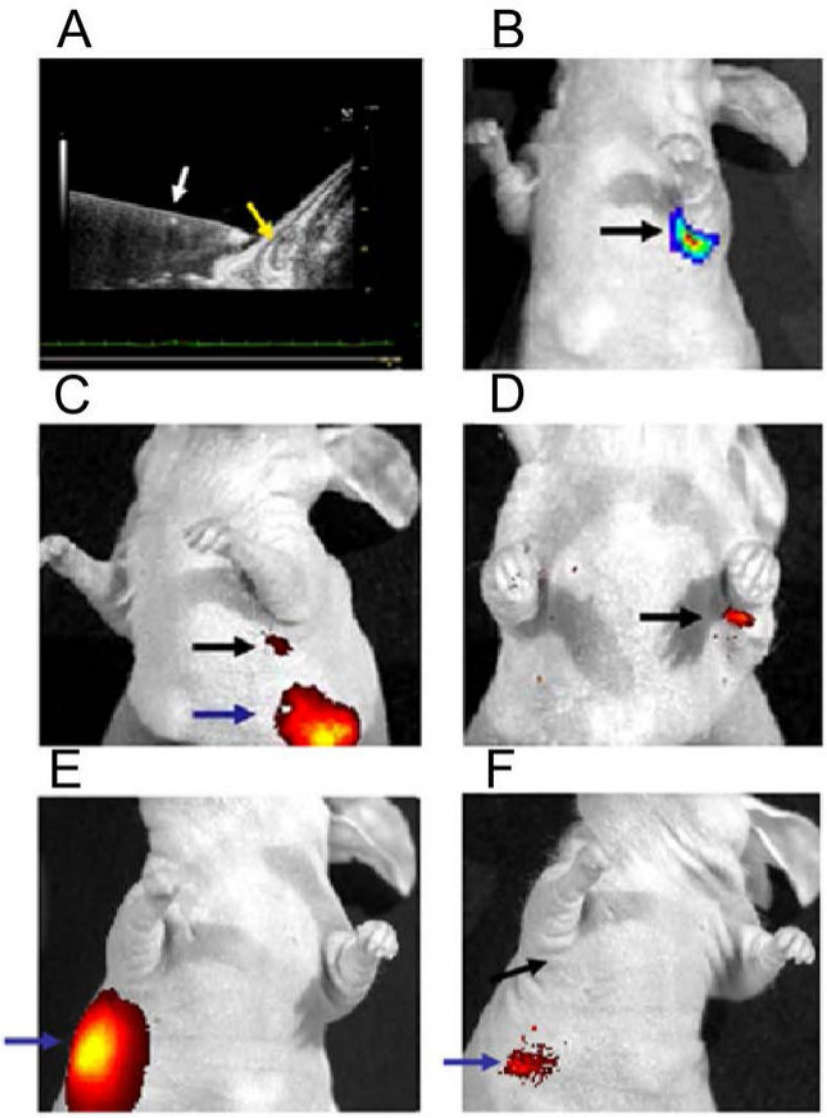

Figure 5.

Ultrasound guided injection of cells into ALN. (A) Axillary node (yellow arrow) and needle (white arrow). (B) Bioluminescence imaging of luciferase expressing cells in axillary node. (C) Fluorescence image of agent injection site (blue arrow) and agent associated with node (black arrow) 24 h after injection. (D) After 7 days, agent is retained in axillary node with positive cells, but has cleared from injection site and other nodes. (E) Fluorescence image of animal injected with 1×10^6 mammaglobin-A negative cells (MDA-mb-231), 5 mins after MFP injection of MamAb-680 (blue arrow). (F) Fluorescence image of the MDA-mb-231 injected node, 24 h post MFP injection of agent. No signal is detected in the area of the ALN (black arrow).

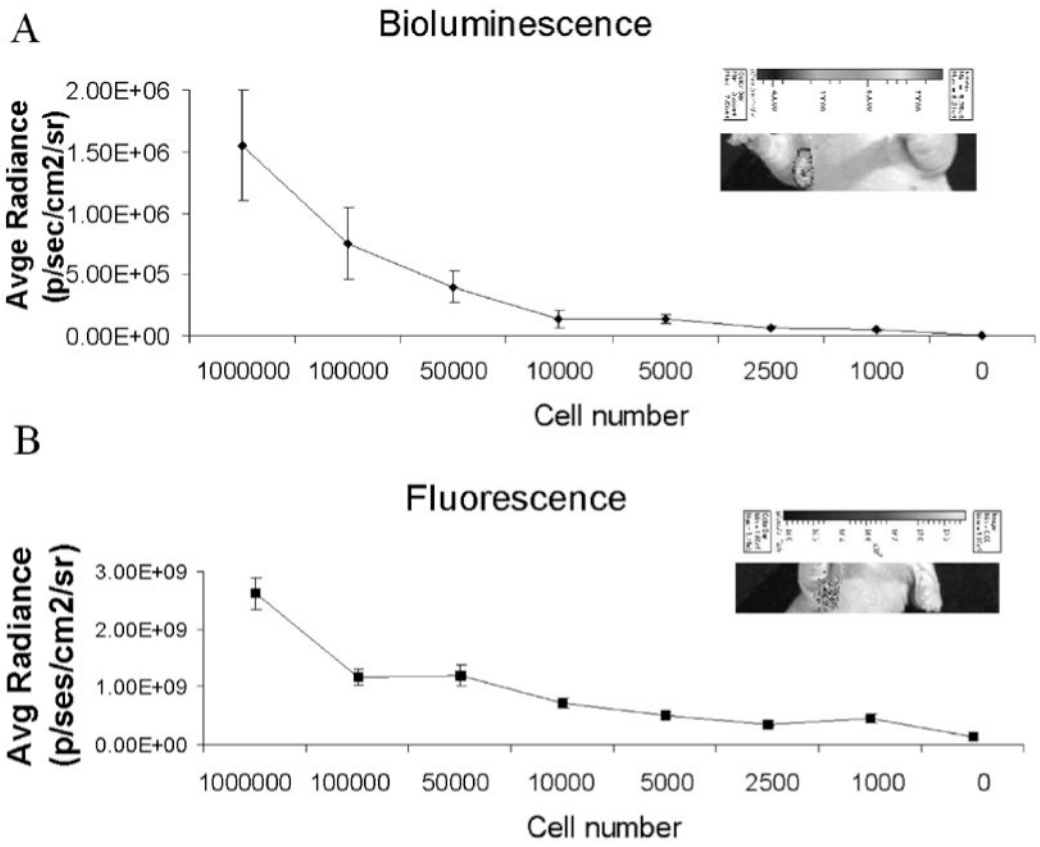

Figure 6.

Sensitivity of detection of cells injected into the ALN. (A) Bioluminescence activity quantified for a range of injected cell numbers. Inset shows signal for a mouse injected with 1000 cells. (B) Agent associated fluorescence for a range of cell numbers, 24 h post-injection with MamAb-680. Inset shows fluorescence for a mouse injected with 1000 cells. All data represent mean ± s.d. of pixel values within the ROIs.